FATIGUE LIFE EVALUATION OF THE DIEFENBAKER BRIDGE USING STRUCTURAL HEALTH MONITORING

Morgan, C.J.[1,2,3], Sparling, B.F.[1], Wegner, L.D.[1]

[1] University of Saskatchewan, Canada

[2] WSP Canada Inc.

[3] chrismorgan1714@gmail.com

Abstract: A structural health monitoring system was installed on the Diefenbaker Bridge, located in Prince Albert, Saskatchewan, to refine an estimate of its remaining fatigue life. The 304 metre long, seven span bridge consists of two separate fracture critical superstructures, each comprising a cast-in-place concrete deck supported by two non-composite welded wide flange girders. Previous studies, based solely on a structural analysis, concluded that the connection of the lateral bracing to the girder web had less than five years of remaining fatigue life. Due to the uncertainty involved in this calculation, the data acquired from six months of field monitoring were used to refine the fatigue life evaluation. Three methods were applied to calculate the remaining fatigue life, including a deterministic method, AASHTO's method, and a probabilistic method. Finite element modelling was completed to characterize the three-dimensional stress state at the connection. In addition, fatigue damage accumulated during the monitoring period was calculated and compared on the basis of detail location, traffic direction, day of the week, and month. Lastly, in-situ bridge behaviours, including degree of composite action, lateral load distribution, and dynamic influence, were investigated. Results demonstrated that costly improvements to the connection detail were not required. It was found that the exterior girders are more heavily loaded than the interior girders, the northbound structure is more heavily loaded than the southbound, and Wednesday is the day of the week with the heaviest loading. In addition, unexpected composite action and minimal dynamic load influence were found to exist on the bridge.

1   INTRODUCTION

The Diefenbaker Bridge over the North Saskatchewan River is a vital river crossing that connects the southern region of Saskatchewan with the north. Its importance to the provincial economy is well documented, making every decision regarding its maintenance a high priority. An evaluation and assessment of the bridge that were completed in November 2016 (ISL, 2016) indicated that the fatigue life remaining at the connection of the lateral bracing to the girder web was nearly exhausted. Given the social, political, and economic impacts of this assessment, and the inherent uncertainty involved in the analysis, it was recommended that a structural health monitoring (SHM) system be implemented and used to refine the fatigue life estimate.

2   DESCRIPTION OF THE BRIDGE AND STRUCTURAL HEALTH MONITORING PLAN

2.1   Bridge Description

Constructed in 1959, the bridge consists of two fracture critical superstructures on a shared substructure. As shown in Figure 1, each structure carries two lanes of traffic for a total travelled width of 7.3 metres per

superstructure, and features seven spans for a total length of 304.4 metres. The bridge deck, piers, and abutments are built with cast-in-place concrete, while the girders are welded wide flange sections.

Figure 1: Overview of the Diefenbaker Bridge

2.2   Condition of Bridge and Characterization of Fatigue Detail

The structural detail governing the fatigue life of the bridge is the welded connection between the longitudinal girder web and the horizontal and transverse bracing. Seen in Figure 2, this connection is considered a Category E detail according to CSA S6-14 (CSA, 2014).

Figure 2: Fatigue detail being investigated

The lateral bracing and bottom chords of the transverse bracing are bolted to a gusset plate, with the plate welded to the girder web. As cracks typically initiate in areas of small flaws or imperfections, such as boltholes, welds or changes in cross sections, the termination of the gusset plate weld, as highlighted in Figure 2, was determined to be the probable initiation point of a crack.

Bracing connections to girder webs can be susceptible to distortion induced fatigue. Distortion induced fatigue occurs at this type of detail when out-of-plane web distortions in the gaps between gusset plates occur, causing bending stresses. In the case of the Diefenbaker Bridge, since the transverse stiffener is connected to the gusset plate and the transverse bracing, this detail is much less susceptible to the distortion induced situation (NHCRP 335, 1990).

However, the critical location at the termination of the gusset plate weld is subjected to a complex stress state generated by partially correlated effects due to bending in the girder and axial forces in the bracing members. To relate this three-dimensional stress state to the uniaxial fatigue behaviour assumed by CSA S6-14 provisions, the von Mises stress was calculated using Equation 1 for the fatigue life evaluation:

[1] $\sigma_{\text{VM}} = \sqrt{\frac{1}{2}\left[\left(\sigma_{xx} - \sigma_{yy}\right)^2 + \left(\sigma_{yy} - \sigma_{zz}\right)^2 + \left(\sigma_{zz} - \sigma_{xx}\right)^2\right] + 3\left(\tau_{xy}^2 + \tau_{yz}^2 + \tau_{zx}^2\right)}$

where σ_{xx}, σ_{yy} and σ_{zz} are the normal stresses in longitudinal, transverse, and vertical directions respectively, and τ_{xy}, τ_{yz} and τ_{zx} are the shear stress components. The maximum distortional energy theory (i.e., von Mises) applies to ductile, isotropic materials, such as steel, that are subjected to complex stress states, and works well with any complex three-dimensional loading condition (Beer et al., 2009).

2.3   Bridge Instrumentation

The primary objective of the monitoring plan was to refine the fatigue life estimate for the bracing connection to the girder web. By instrumenting the bridge as shown in Figure 3, important data could be collected, including the following:

•Stress Magnitudes – the stress history, and therefore the fatigue life, are highly dependent on the traffic volume and the weight of trucks that cross the bridge. From a historical perspective, this information is very difficult to quantify; however, an understanding of current loading conditions and their associated stress ranges increases the accuracy of the analysis, with the possible outcome of reducing the potential for unnecessary repairs and improvements; and

•Stress Distribution and Cycles – in addition to the magnitude of the stresses, the locations of high stress and the number of cycles that occur were established. This narrowed the scope of weld improvements that had to be considered, as the measured data identified which of the two superstructures and which particular connection locations were more heavily loaded. This information was also important when determining service life estimates and maintenance plans, as it can be used to avoid over-investment in non-essential repairs by allowing a more targeted approach to be taken.
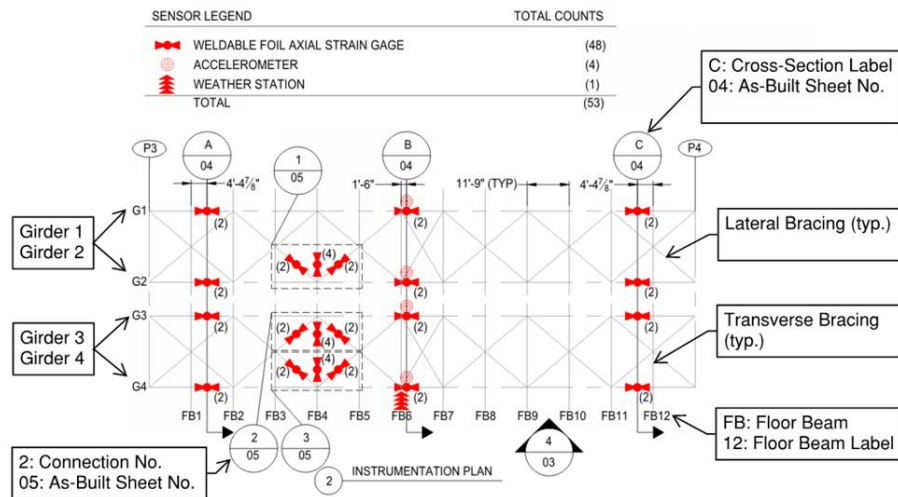

Figure 3: Instrumentation Plan

Sensors were strategically placed along Span Four (i.e., the central span) such that equipment and installation effort was minimized without compromising the quality of data. For simplicity, the instrumentation plan can be broken down into two categories that include girder instrumentation and connection instrumentation. The purpose of the girder instrumentation was to provide insight into the global behaviour of the bridge so that a finite element model could be calibrated. Uniaxial strain gauges were installed in the longitudinal direction on the top and bottom of all four girder webs at Cross Sections A, B, and C, as seen in Figure 3, to monitor the peak positive and negative bending moment regions. All sensors were strategically located away from the anticipated neutral axis of the girders to maximize the strain measurements, and therefore, the signal-to-noise ratios.

The purpose of the connection instrumentation was to acquire data that could be used to determine the stress distribution and magnitudes within the critical fatigue detail. Uniaxial strain gauges were installed on the lateral and transverse horizontal bracing members connected to the gusset plate.

2.4 Data Acquisition

2.4.1 Calibration Data

Calibration data were acquired by removing all traffic from the structure and driving a truck of known weight across in a controlled manner. The truck shown in Figure 4 was supplied by the Saskatchewan Ministry of Highways and Infrastructure, and was used to perform the calibration loading. A minimum of two trials per lane with controlled speeds were completed, with one additional slow median lane trial completed per direction. Completing at least two trials per test allowed the team to validate the quality of the data.

Data were acquired during the slow speed passes (10 km/hr) at 50 Hz and at 100 Hz for the high speed passes (50 km/hr). By performing multiple passes in each lane and at each speed, the quality of the data could be verified. Data quality indicators include reproducibility, elastic behaviour (i.e. strains returning to zero after trial), symmetry of responses, and lack of noise.

Figure 4: Calibration Vehicle

2.4.2 Rainflow Data

The cycle counting algorithm used to acquire uncontrolled traffic data was set up according to the rainflow counting method described in ASTM E1049. This method is well suited for variable amplitude fatigue loading since it identifies stress ranges associated with closed-loop hysteresis. The selected ranges of stress were based on the maximum values experienced during the calibration loading. Recognizing that larger stress ranges may be experienced, the ranges were set up in 5 MPa increments up to 30 MPa. Small ranges of less than 2.5 MPa were omitted as this range would experience a large number of cycles due to the presence of noise and would contribute minimally to fatigue damage.

3 OVERVIEW OF ANALYSIS METHODS

3.1 Finite Element Modelling

The gusset plate connection to the girder web experiences forces applied from varying directions, causing a three-dimensional stress state. The potential sources of the stress include the bottom leg of the lateral bracing, the bottom and top legs of the transverse bracing, as well as flexural and shear stresses in the girder. Since the point of interest (POI) at the weld termination on the gusset plate could not be instrumented directly, its stress state was estimated based the measured responses in the members to which it was connected.

Adding to the challenge, the number of cycles in each stress range at the POI had to be inferred based on the stress variations and load cycles being applied from these various sources that were not necessarily acting in perfect unison. However, a statistical comparison between calibration test data sets comparing the load cycles measured in the girder at Cross Section B and those observed in the bracing in that vicinity revealed a correlation coefficient (R^2) of 0.99, indicating that there was a very strong correlation in the number of load cycles from the two data sets. This result is reasonable since a particular load cycle experienced on the girder at Cross Section B is typically caused by the same load event that induces a load cycle in the bracing at the POI. Therefore, for the fatigue evaluation, the number of load cycles experienced at the POI for the various connection locations was assumed to be identical to the number of cycles measured by the bottom strain gauge at Cross Section B.

Since the instrumented connections were located at some distance away from the instrumented girder locations (see Fig. 3), stresses in the girder at the POI could not be determined directly from test data. As a result, two separate finite element models were developed to provide more detailed information on stress distributions in the various bridge components. First, a comprehensive finite element model of one of the two bridge superstructures was generated to investigate girder flexural and shear stresses in the vicinity of the POI. Subsequently, a detailed finite element model of an isolated connection was used to determine the contribution that forces in the lateral and transverse bracing had on the stress state at the POI.

The comprehensive superstructure model was developed using the commercial software SAP 2000 (CSI., 2019) as part of a parallel research project investigating the application of vibration-based damage detection to this bridge (Castillo, 2019). The comprehensive model was calibrated against measured calibration test data by adjusting model parameters including the degree of composite action between the girders and deck, interaction of the barrier with the deck, support conditions, and the elastic modulus of concrete, until satisfactory agreement was obtained. Using the calibrated finite element model, simulated truck loading events with live load amplitudes scaled to produce responses matching the levels associated with each of the predefined "rainflow bins" used in the fatigue analysis were then applied to extract the corresponding girder flexural and shear stress at the POI location.

The isolated connection finite element model was created based on as-built drawings and field-tested material properties using ANSYS Simulation Software (ANSYS Inc., 2019). The connection model featured a 2 meter long segment of the bridge girder with an attached gusset plate that was loaded by concentrated axial forces from the various bracing members at their connection points. Rainflow data collected from the connection instrumentation was used to define stress ranges in each bracing member associated with each of the predefined "rainflow bins". Since the distribution of stress cycles in the lateral and transverse bracing elements at a given connection was found to be very similar (with a correlation coefficient of 0.99), it was assumed that peak stresses within each stress range occurred simultaneously in all bracing elements (i.e., when a 15 MPa stress was induced in the lateral brace, the same 15 MPa stress was induced at the transverse brace). Based on that assumption, stress components at the POI associated with each applied stress range could be extracted.

Since the transverse and lateral bracing cycles correlated closely with the girder cycles for each stress range, they were assumed to act simultaneously for the purposes of the fatigue analysis. The three-dimensional stress state was then deduced from the stress components extracted from the two finite element models, allowing the von Mises stress [Eq. 1] at the POI to be calculated for each stress range.

3.2 Fatigue Life Evaluation

Since the stress on bridge structures is variable, a cumulative damage rule is required to relate this variable amplitude stress to the constant amplitude fatigue data used to derive commonly used design specifications. The stress-based approach to fatigue utilizes a relationship between constant amplitude stress (S) and the number of stress cycles (N). Many specifications have adopted this approach, including CSA S6-14 (CSA, 2014). The Palmgren-Miner linear damage hypothesis, also called Miner's Rule, relates the variable amplitude loading commonly found on bridge structures to the S-N relationships derived from the fatigue experiments. Miner's rule is one of the most widely used damage accumulation rules, and is shown in Equation 2 (Miner, 1945):

[2] $\qquad D = \sum_{j=1}^{k} \frac{n_j}{N_{f,j}}$

where D is Palmgren-Miner's damage accumulation index, n_j is the number of measured cycles at a specific stress range, and $N_{f,j}$ is the number of cycles until failure at that same stress range. The variable k represents the number of different stress ranges considered.

Multiple stress ranges can be converted into a single, equivalent stress range using Miner's Rule and the concept of effective stress. This is done because a bridge component experiences many different stress ranges, making a summation of the damage contributions impractical (Fasl, 2013). The effective stress

range is calculated using Equation 3 to relate variable amplitude loadings to an equivalent constant amplitude loading:

$$[3] \qquad S_{re} = \left(\frac{\sum n_j \times S_j^3}{N_m}\right)^{1/3}$$

where S_{re} is the effective stress range (MPa), n_j is the measured number of cycles in a bin corresponding to S_j, S_j is average stress for bin j (MPa), and N_m is total number of cycles measured during the monitoring period.

Using the effective stress, the fatigue lives of different details may be compared using a single stress range. This is useful for infrastructure owners because it allows the identification of problems within a single bridge or across an entire bridge inventory.

NCHRP Project 12-15(4) explored fatigue behaviour if the majority of cycles were less than the constant amplitude fatigue limit (CAFL) (Fisher et al.,1983). This study revealed a few important phenomena, such as (a) if any portion of the applied stress was above the CAFL, fatigue cracking would occur, and (b) if no cycles were observed above the CAFL then fatigue cracking did not occur. It was also found that the fatigue life of the detail could be calculated using a straight-line extension of the S-N curve, which suggests that all stress cycles contributed to the damage.

3.2.1   Deterministic Method of Fatigue Life Evaluation

In the deterministic approach to fatigue life evaluation, the damage from specific monitoring periods is used to estimate damage in the past, and to forecast damage in the future. A traffic growth rate is assumed, and damage is accumulated over the service life of the bridge until failure occurs. The fatigue life can be calculated using Equation 4 (Fasl, 2013):

$$[4] \qquad m = \frac{\log\left(\frac{r \times A}{N_{yk} \times S_r^3} \times (1+r)^{(k-1)} + 1\right)}{\log(1+r)}$$

where m is the fatigue life in years, r is the annual increase in traffic volume, N_{yk} is the current traffic volume per year, k is the current age of the bridge, S_r is the stress range, and A is detail fatigue constant (MPa).

If the mean value for the fatigue constant is used in place of the design value (A), the mean fatigue life can be calculated. The design value will produce a probability of failure of 5% (95% confidence interval), whereas the mean value will correspond to a probability of failure of 50%. Since the stress range and traffic volume correspond to the current year, the effective stress range can be used along with the corresponding number of cycles.

3.2.2   AASHTO Method of Fatigue Life Evaluation

The remaining fatigue life can also be calculated using the method outlined in AASHTO's Manual for Bridge Evaluation (2011). To provide a consistent level of reliability, different partial load factors are recommended based on how the effective stress range was calculated. Since field data were used to calculate the remaining fatigue life, Equation 5 from NCHRP Project 12-81 was used:

$$[5] \qquad Y = \frac{\log\left(\frac{(R_R \times A \times g(1+g)^{a-1})}{365 \times n \times \left((\Delta_f)_{eff}\right)^3 \times [(ADTT)_{SL}]_a} + 1\right)}{\log(1+g)}$$

where Y is the fatigue life in years, g is the annual traffic growth increase, n is the number of cycles per truck passage, a is the current age of the bridge, $(\Delta_f)_{eff}$ is the effective stress range, $(ADTT)_{SL}$ is the average number of trucks per day in year a, R_R is the resistance factor for desired probability of failure, and A is detail fatigue constant (MPa).

3.2.3 Probabilistic Method of Fatigue Life Evaluation

Uncertainty in material strength, section dimensions, loading, bridge response, and many other sources, make estimating the remaining fatigue life of a detail on a bridge very challenging. Structural reliability is a method that can characterize the probability of failure with consideration of the uncertainty involved. The NCHRP Project 12-28(03) by Moses et al. (1987) developed an approach that provided a consistent level of reliability for typical of bridge types under certain conditions. The methodology outlined in Fasl et al. (2013) was followed to perform the probabilistic evaluation of the remaining fatigue life.

3.3 In-Situ Behavior Characterization

Girder bending moments caused by the calibration loading trials were estimated from the measured girder strain profiles using a transformed section analysis. The lateral distribution of bending moments between the two girders was then determined for the calibration loading using Equation 6:

[6]   Lateral Load Distribution $= \dfrac{M_i}{\sum_{i=1}^{2} M_j}$

where M_i is the calculated moment corresponding to the strain response at midspan, and $\sum M_j$ is the sum of the calculated moments for both girders at midspan. The dynamic load allowance (DLA) was calculated based on the peak static strain response (slow passes), $\epsilon_{static,}$ and dynamic strain response (fast passes), $\epsilon_{dynamic}$, from the calibration loading using Equation 7:

[7]   DLA $= \dfrac{\epsilon_{dynamic}}{\epsilon_{static}}$

4 ANALYSIS AND RESULTS

4.1 Fatigue Damage Accumulation

The amount of damage per day, per month, per connection, and per direction of travel was characterized and compared. The total damage could be divided by the fatigue detail constant (A) to calculate the damage accumulation index, but since all details being compared belonged to the same category, the result of the comparison would be the same – just at a different scale.

The average damage per day, and per girder, is summarized in Figure 5. While only Girders 2, 3 and 4 had instrumented connections, the behaviour of Girders 1 and 4 (i.e., exterior girders) and Girders 2 and 3 (i.e., interior girders) were found to behave with near symmetry. Therefore, using the calibrated finite element model, the connection on Girder 1 was also evaluated since strain data at midspan on the girder were available. This allowed the comparison of behaviour between the northbound structure (Girders 3 and 4) and the southbound structure (Girders 1 and 2).
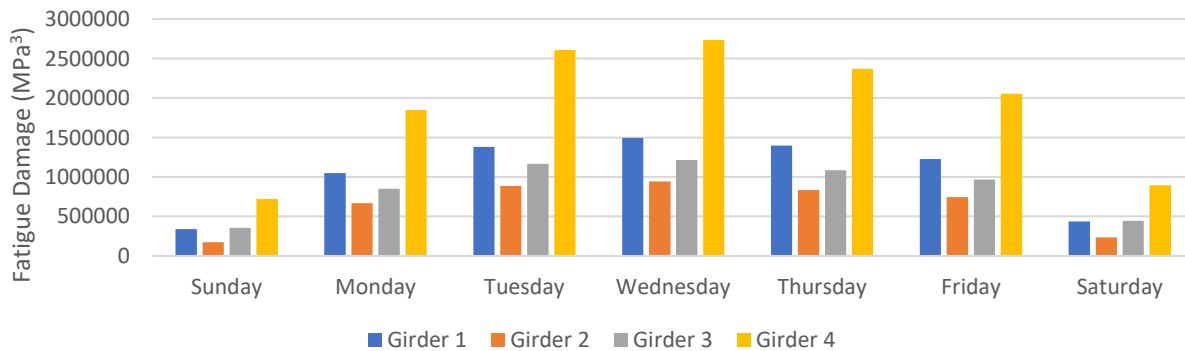

Figure 5: Average Daily Damage Accumulation

The connection on Girder 4 (exterior girder on northbound superstructure) experienced the most fatigue damage with the connection on Girders 1, 2 and 3 receiving 54%, 32%, and 47% of the damage on Girder 4, respectively. The northbound structure experienced 38% more damage than the southbound structure. Wednesday contributed the most damage on average, with the daily contributions progressively lessening as the day nears the weekend. By normalizing the data by the number of days per month, the relative amounts of damage per month were also explored, as shown in Figure 6.
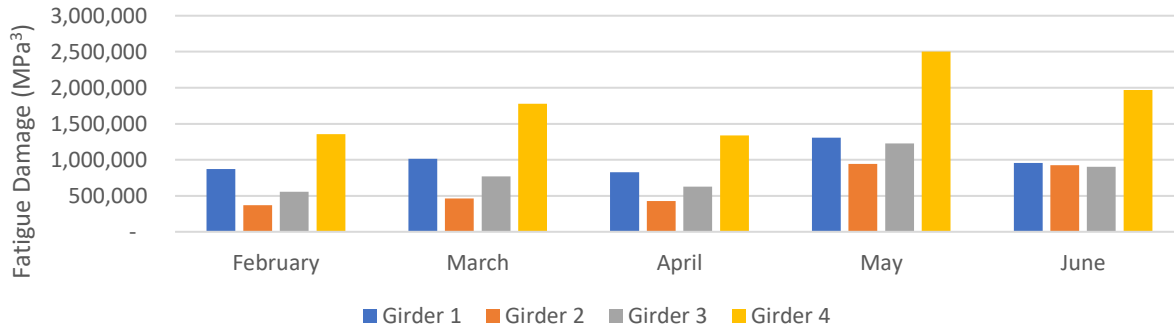

Figure 6: Average Daily Fatigue per Month

The exterior girders sustained more damage than the interior girders, with Girder 4 being the most damaged. May was the most heavily loaded month, with the remaining months contributing similar amounts of damage.

4.2   Remaining Fatigue Life

Using the stress components obtained from the finite element models, the equivalent von Mises stresses at specified connections were calculated, based on the rainflow data acquired at Cross Section B, and used to calculate the remaining fatigue. Results are summarized in Table 1. The annual growth rates shown in this table were the assumed rates of increase in traffic volume.

Table 1: Calculated remaining fatigue life using the deterministic, AASHTO, and probabilistic approaches

P_f*	Remaining Fatigue Life at Connection 1 (years)			Remaining Fatigue Life at Connection 3 (years)		
	Deterministic	AASHTO	Probabilistic	Deterministic	AASHTO	Probabilistic
2% Annual Growth						
5%	151	176	240	102	126	189
16%	-	185	264	-	135	214
33%	-	193	284	-	143	234
50%	173	175	300	123	125	250
4% Annual Growth						
5%	93	106	138	68	80	113
16%	-	110	151	-	85	125
33%	-	114	161	-	89	135
50%	104	105	169	79	80	145
6% Annual Growth						
5%	69	78	100	52	61	83
16%	-	81	108	-	64	91
33%	-	84	115	-	66	98
50%	77	77	120	60	60	103

*P_f – Probability of Failure

The deterministic and AASHTO methods show strong agreement, with the probabilistic method producing the longest estimated remaining fatigue life. Under the most conservative (6%) traffic growth scenario and probability of failure (5%), these results suggest that at least 52 years of fatigue life remain on this detail.

4.3 In-Situ Behaviour Characterization

4.3.1 Degree of Composite Action

To quantify the degree of composite action that is occurring, a transformed section analysis of the girder and deck was undertaken in which the effective area of concrete was varied until the theoretical neutral axis aligned with the location based on measured girder strain profiles. While it could not be established with certainty what portion of concrete was contributing to composite action, it can be concluded that, at the very least, portions of the deck and barrier, and perhaps a portion of the sidewalk, were contributing to the composite action of the section for Girder 1 (exterior girders). Using a similar approach for Girder 2 (interior girders), it was found that Girder 2 is acting compositely with the deck, with neutral axis being located approximately 50% higher than would be expected for a non-composite system.

4.3.2 Lateral Load Distribution

With effective section properties established using the approach described above, nominal midspan bending moments resisted by each girder were calculated based on measured strain data from the calibration load tests. Applying Eq. 6, lateral load distribution factors could then be determined. On that basis, it appears that more load sharing is occurring between girders than is typically suggested by commonly used simplified approaches. For example, Table 2 presents a comparison of lateral load distributions derived from the current test data and the static apportioning method in which the bridge deck is treated like a simply supported beam supported on two girders (Bakht et al., 2015).

Table 2: Summary of lateral load distribution at mid-span

	Actual		Static Apportioning Method	
	Barrier Lane Test	Median Lane Test	Barrier Lane Test	Median Lane Test
Exterior Girder	65%	42%	82%	11%
Interior Girder	35%	58%	18%	89%

4.3.3 Bridge Dynamics

The average dynamic load allowance (as per Eq. 7) from the calibration loading tests was found to be 1.006. This is significantly less than the value of 1.25 prescribed in CSA S6-14, indicating that there was not a significant dynamic effect observed. It should be noted, though, that the current test program considered only a single loaded lane, while the value in CSA S6-14 considers the possibility of multiple simultaneously loaded lanes.

5 CONCLUSIONS

Based on the structural health monitoring results from the Diefenbaker Bridge, the following significant conclusions can be made:

1   The remaining fatigue life estimate was increased from five years (based on structural analysis only), to at least 52 years. Since fatigue of the critical detail is therefore unlikely to govern the service life of the structure, this conclusion saved the owner from a costly investment in fatigue detail improvements.

2   Understanding how the structure is loaded (i.e., the northbound structure experiences more damage than southbound, exterior girders experience more damage than interior, etc.) will allow the owner to target maintenance plans and inspections effectively. These damage trends also indicate that the structure's loading is commercially driven; therefore, permitting costs could be adjusted accordingly.

3   Full composite behaviour between the steel girders and concrete deck was found to occur, despite the absence of mechanical attachment between the deck and girder. In addition, insignificant dynamic load influence was found during the calibration loading and increased lateral live load distribution was found to exist. While these behavioural characteristics cannot be relied upon at ultimate limit states without further load testing, they provide an added level of comfort to existing load evaluations.

6   ACKNOWLEDGEMENTS

7   REFERENCES

AASHTO. 2011. *The Manual for Bridge Evaluation.* 2nd Edition. American Association of State Highway and Transportation Officials. Washington, DC. USA.

ANSYS Inc. 2019. *ANSYS Simulation Software, Version 19.* Delaware, USA.

ASTM. 2011. *E1049-85: Standard Practices for Cycle Counting in Fatigue Analysis.* ASTM International. West Conshohocken, PA, USA.

Bakht, B., and Mufti, A. 2015. *Bridges – Analysis, Design, Structural Health Monitoring, and Rehabilitation.* 2nd Edition. Springer International Publishing. Switzerland

Beer, F., Johnston, E., Dewolf, J., Mazurek, D. 2009. *Mechanics of Materials.* 5th Edition. McGraw-Hill, New York, NY, USA.

CSI. 2019. *SAP 2000 Integrated Software for Structural Analysis and Design.* Computers and Structures Inc. Berkeley, California, USA.

CSA. 2014. *CAN/CSA S6-14, Canadian Highway Bridge Design Code.* Canadian Standards Association, Rexdale, Ontario, Canada.

Castillo, J. 2019. *An Investigation into the Effects of Damage on the Diefenbaker Bridge* [in progress]. University of Saskatchewan. Saskatoon. Saskatchewan. Canada.

Fasl, J. 2013. *Estimating the Remaining Fatigue Life of Steel Bridges Using Field Measurements.* The University of Texas at Austin. Dissertation.

Fisher, J., Mertz, D., and Zhong, A. 1983. *Steel Bridge Members Under Variable Amplitude Long Life Fatigue Loading.* Transportation Research Board. National Research Council. Washington, D.C. USA.

ISL Engineering and Land Services. 2016. *Diefenbaker Assessment and Evaluation Report.* Saskatchewan Ministry of Highways and Infrastructure. Saskatoon. Saskatchewan. Canada.

Miner, M. 1945. *Cumulative Damage in Fatigue.* Journal of Applied Mechanics, 12, A159-A164.

Moses, F., Schilling, C., and Raju, K. 1987. *Fatigue Evaluation Procedures for Steel Bridges.* Transportation Research Board. National Research Council. Washington, D.C. USA.

National Cooperative Highway Research Program. 1990. *Distortion Induced Fatigue Cracking in Steel Bridges, NCHRP Report 336,* Transportation Research Board, National Research Council, Washington, DC. USA.